

Multiscale modelling of desquamation in the interfollicular epidermis

Claire Miller ^{1[#],2[#],3}, Edmund Crampin ^{2,4,5}, James M. Osborne ^{1*},

1 School of Mathematics and Statistics, The University of Melbourne, Parkville, Victoria 3010, Australia

2 Systems Biology Laboratory, School of Mathematics and Statistics, and Department of Biomedical Engineering, The University of Melbourne, Parkville, Victoria 3010, Australia

3 Computational Science Lab, University of Amsterdam, 1098 XH Amsterdam, Netherlands

4 School of Medicine, Faculty of Medicine, Dentistry and Health Sciences, The University of Melbourne, Parkville, Victoria 3010

5 ARC Centre of Excellence in Convergent Bio-Nano Science and Technology, Melbourne School of Engineering, The University of Melbourne, Parkville, Victoria 3010, Australia

* jmosborne@unimelb.edu.au

Former position where most of work was done.

Abstract

Maintenance of epidermal thickness is critical to the barrier function of the skin. Decreased tissue thickness, specifically in the stratum corneum (the outermost layer of the tissue), causes discomfort and inflammation, and is related to several severe diseases of the tissue.

In order to maintain both stratum corneum thickness and overall tissue thickness it is necessary for the system to balance cell proliferation and cell loss. Cell loss in the epidermis occurs when dead cells at the top of the tissue are lost to the environment through a process called desquamation. Cell proliferation occurs in the basal layer and causes constant upwards movement in the tissue.

In this paper we will investigate combining a (mass action) subcellular model of desquamation with a three dimensional (overlapping spheres) multicellular model of the interfollicular epidermis. The model shows that hypothesised biological models for the degradation of cell-cell adhesion from the literature are able to provide a consistent rate of cell loss in the multicellular model, which balance proliferation, hence maintaining a homeostatic thickness. We also use the model to investigate the effect of having two proliferative cell types with different proliferation rates in the basal layer, determining that it is possible to reproduce the same tissue dynamics with a single cell type population with rate equal to the harmonic mean of the two populations. An investigation into a disorder which disrupts this desquamation model shows reduced tissue thickness, consequently diminishing the protective role of the tissue, and two treatment hypotheses are compared.

Author summary

We are interested in understanding how the thickness of the epidermis—the outer layer of the skin—is maintained. Maintaining a sufficient thickness is critical to skin, and generally whole body, health. To do this, we combine mathematical models of processes occurring to and between cells in the epidermis, and the processes occurring at a smaller scale that cause them, to understand the relationship between the two scales and their role in epidermal thickness. More specifically, it is broadly accepted that the loss of skin cells from the top of the epidermis is due to a gradual reduction in the adhesion between connecting cells as they move upwards through the epidermis. We look in further detail at what is causing this decrease in adhesion, and at the balance between the loss of adhesion, resulting cell loss, and creation of new cells in the lower layers of the epidermis.

Introduction

The outermost layer of the skin, the epidermis, a layered epithelial tissue, provides our bodies from protection from external hazards, in part through the constant turnover of cells. This is thought to assist in flushing out any toxins which may have entered the system. Due to this turnover, the tissue fully renews roughly every 4 weeks [1] and requires a balance of cell input and output in order to maintain a homeostatic tissue thickness. The thickness of the epidermis varies both between body location and individual, ranging from 50 to 100 μm [2, 3].

The most superficial layer of the epidermis is the stratum corneum (or just corneum). This layer is critical to cell turnover, as it is from the top of the layer that cells are lost through a process known as desquamation. Desquamation refers to the shedding of the cells in clumps (squames) from the surface of the skin, and is associated with a reduction in cell-cell adhesion towards the top of the tissue. Excessive desquamation, or peeling, of the epidermis causes deficiencies in barrier function of the skin. This allows the ingress of antigens, resulting in inflammation and has been linked to allergic diseases such as atopic dermatitis (eczema), food allergies, or asthma [4, 5]. Diseases of the skin can range from a nuisance to a major health risk, with debilitating or even fatal consequences, and even the less severe diseases can have flow on effects for our health.

The subcellular biology of desquamation

A critical part of the desquamation process is the degradation of cell-cell adhesion. Throughout the lower layers of the epidermis, the cell-cell adhesion is due to protein complexes called desmosomes. When the cell transition into the stratum corneum, the desmosomes become corneodesmosomes through the addition of corneodesmosin. As the cell proceeds upwards through this final layer, these corneodesmosomes are degraded via an assortment of proteases (enzymes that break down proteins) [6, 7]. The transition and degradation of cell-cell adhesion is shown in Figure 1.

As illustrated in Figure 1, the degradation of the corneodesmosomes is not uniform around the circumference of the cell—it occurs first in the vertical direction on the horizontal surfaces of the flattened cells, and then in the planar direction. This delayed degradation in the planar direction is potentially due to the presence of other adhesion protein complexes called tight junctions, which potentially limit access to the the corneodesmosomes by the proteases [8].

The specific protease subgroup that are known to degrade the proteins in the corneodesmosomes are kallikrein serine proteases, or KLKs [4, 5, 7, 9]. These KLK enzymes are released by the cell into extracellular space at the base of the corneum (via

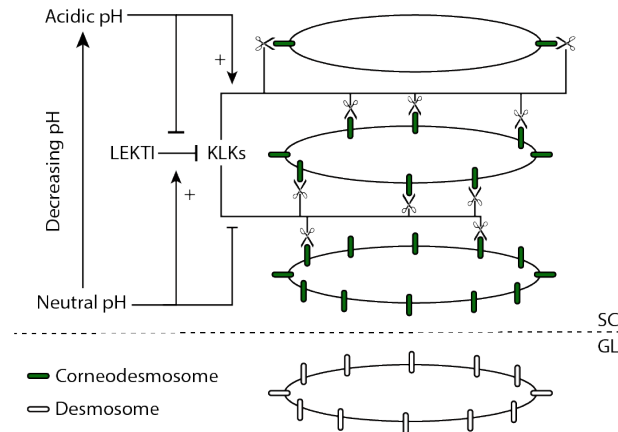


Fig 1. A diagram representing the involvement of pH, LEKTI, and KLKs in the desquamation process. Desmosomes (white ellipses) are converted to corneodesmosomes (green ellipses) as they enter the stratum corneum (SC in figure) from the granular layer (GL in figure). These corneodesmosomes are then degraded by KLKs, first on the horizontal surfaces then the vertical (indicated by the scissors). The degradation process is inhibited by LEKTI, which binds with the KLKs and stops the KLKs from binding with the corneodesmosomes. The local pH regulates the inhibition, as well as the corneodesmosome degradation rate by KLKs. Arrows with ‘+’ symbols indicate the pH increases the reaction, while ‘-’ indicates an inhibitive reaction or that the pH reduces the rate of a reaction.

lamellar bodies) [5,6]. Other families of proteases are also known to contribute to degradation, however we only consider KLK proteases as they are thought to be the primary enzyme, and are consequently the most studied [5,10,10,11]. The data available on this process is mostly limited to KLK5 and KLK7 [5,10]. KLK5 constitutes around 10% of the proteases and KLK7 constitutes 36%. However, KLK5 is a trypsin-like KLK while KLK7 is chymotrypsin-like. The remaining 54% of KLKs are all trypsin-like, and therefore we assume KLK5 has properties more representative of the majority than KLK7. As a result, for simplicity, we focus on KLK5 in this study and assume it is representative of all KLK protease activity.

The final pieces of the puzzle shown in Figure 1 are the inhibitor LEKTI and the pH gradient. In addition to KLK proteases, the lamellar bodies also secrete LEKTI which is an inhibitor to the reaction between the KLK proteases and the corneodesmosomes [11–13]. The effectiveness of LEKTI at inhibiting the KLK-corneodesmosome reaction is regulated by the local pH, which varies vertically through the corneum. The pH gradient changes from neutral in deep corneum to acidic in superficial corneum [14]. At neutral pH (deep corneum) there is a high level of interaction between LEKTI and KLK, while low pH (superficial corneum) increases dissociation of LEKTI and KLK, allowing for higher rates of corneodesmosome degradation [5].

In addition to regulating the LEKTI/KLK interaction, the pH also directly contributes to regulation of the degradation process. At neutral pH (deep corneum) the rate of degradation of the corneodesmosomes by the KLK protease is thought to be lower than that at low pH (superficial corneum). These interactions are all summarised in the diagram shown in Figure 1.

Multiscale models of the epidermis

In this paper we are interested in developing a multiscale model of the epidermis which incorporates a subcellular model of desquamation into a multicellular model of the tissue. There is a long history of overlapping spheres models of the epidermis, beginning with a 2D model from 1995 [15]. This early model incorporated subcellular processes by including an inverse square law to approximate the spread of signalling factors from cells. Over the following decades such models have become more sophisticated, expanding to three dimensions and incorporating more specific subcellular information.

A common approach to multiscale epithelial tissue models is the inclusion of a subcellular ODE model for each cell [16]. For the epidermis, this approach has been used to investigate the role of TGF- β (transforming growth factor β : a signalling molecular thought to help regulate division and differentiation) in wound healing using a mass action model for the subcellular ODE [17, 18]. An alternative subcellular ODE model is a phenomenological ODE model. For example, as the model of calcium waves from [19] which been used in a multiscale model to understand calcium's role in epidermal homeostasis [20].

Another subcellular model that has been previously used to study the calcium gradient in the epidermis is a molecular exchange model. Such a model incorporates the exchange of water and accompanying molecules, such as calcium, between adjoining cells. [21] first implemented this in a 2D multiscale model to show the gradients could generate a flat epidermal surface from an undulating membrane and produce realistic turnover times and calcium gradients. Then [22] extended it to a 3D ellipsoidal model, to show such a system could maintain the calcium gradient itself and generate realistic tissue morphologies.

Another form of multiscale model that has been for the epidermis is a multicellular-extracellular model. For example, the inclusion of an extracellular reaction-diffusion model of nutrients and water to regulate division timing. This model was used to investigate the persistence of melanoma cells in the epidermis under different parameter combinations [23].

In this study we are interested in incorporating a subcellular model of the desquamation process described above into our multicellular model from [24]. Previous models of the epidermis, including a couple of the multiscale models mentioned, have incorporated degradation of cell-cell adhesion for desquamation [22, 23, 25]. However, all these studies only included degradation effects at a cellular level—no previous study has looked in detail at modelling the subcellular processes controlling adhesion degradation. In this study, we implement the hypothesised subcellular biology of desquamation, described above and shown schematically in Figure 1, using a mass action model. We show the results for this model at the subcellular scale for a single cell, highlighting the dynamics occurring as a cell migrates through the epidermis. We then investigate the desquamation process and epidermal homeostasis with a coupled subcellular-multicellular model.

Results

We begin by presenting a model of a single cell which implements the ODE system for the degradation of adhesion. We then incorporate the subcellular model into a multicellular model of the epidermis [24] and consider the multiscale system for a healthy tissue, showing that it is able to maintain a steady state height. Given the proliferation in the epidermis is not completely understood [26–28], we investigate how the presence of two types of proliferative cells would affect the tissue height. Finally, we are interested in the multiscale systems response to a disease, in this case we look at

Netherton syndrome in which the levels of inhibitor (LEKTI) are lower. We consider both a system in which all cells have the same concentration of LEKTI, and a system in which a proportion of the cells have a lower concentration and the remaining cells have a healthy concentration. Both of these investigations hypothesise the possible effect of treating the condition; either by increasing LEKTI levels in all cells, or for a case in which only some cells were treated and others remained diseased.

Realistic adhesion degradation rates in the subcellular model require an effective concentration of enzyme

Using the pathways in Figure 1 a mass action kinetics model was developed to predict the proportion of corneodesmosomes (CND) remaining as the cell moves upwards through the corneum. We track the levels of KLK, LEKTI, and CND in the cell, which change according to a set of mass action based ODEs determined for the system shown in Figure 1. This model uses cell height to determine the local pH, and consequently the rate parameters for the KLK-CND and KLK-LEKTI interactions. The output of interest for this model is the proportion of remaining CND, and this will be used to couple the model to a multicellular system. A full description of the model is given in the Model section, and parameters given in Table 1. Details on the parameterisation are given in S1 File.

The subcellular model is developed for use in a multiscale model of the epidermis, however first we will investigate the model dynamics for a single cell moving upwards through the stratum corneum. We assume that the cell velocity is approximately constant through the corneum stratum, and estimate the migration time as 20 days [29]. This gives us an approximate upwards velocity, normalised by corneum stratum thickness, of $v_\xi = 0.05 \text{ day}^{-1}$. We define xi to be the vertical dimension, normalised by corneum height, and beginning at the interface between the corneum and the lower epidermis. Results showed the system parameters we determined using the literature produced desquamation significantly faster than expected (see S2 File for these results). This indicates that either the rate parameters are wrong (k_{+1} and k_2), or that the mechanism is wrong.

We know many other processes and structures occur in the system that we ignore, which highly likely affects the reaction. In particular, it has been hypothesised that tight junctions at the peripheral of the cells act as a barrier to the enzyme-corneodesmosome interaction at peripheral sites [8]. Additionally, similar effects may be occurring at the central regions of the cell, with the diffusion of the enzyme potentially limited by the intact corneodesmosomes themselves or the lipids that also reside in the extracellular space. Our results indicate that, assuming the determined rate parameters are of the right order of magnitude, this could have a significant effect on the degradation rate. By limiting the diffusion of the enzyme, the system is no longer mixed and consequently the mass action model does not hold.

In order to compensate for this limited diffusion effect, without incorporating complex new processes in the model, we instead propose the use of an *effective concentration of enzyme*. Limited diffusion would reduce the amount of available enzyme to bind to the substrate. Decreasing e_T has the same effect, and consequently this is a way to simulate limited diffusion in a computationally efficient way. Decreasing e_T directly affects the effective rate parameter for the degradation of s , which is given by $k_{+1}e_T$. Note, for simplicity, we also keep $i_T = e_T$. A full investigation into the desquamation rate and the effect of all the reactant concentrations is given in S2 File. Figure 2 shows a reduced concentration of e_T is able to reproduce the rates expected for the desquamation process.

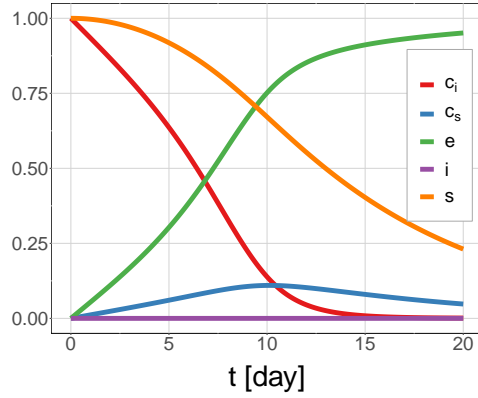


Fig 2. Solution of the subcellular model for a cell moving at a specified velocity through the pH gradient of the corneum, using an effective concentration of KLK enzyme: $s_0 = 10 \mu\text{M}$, $e_T = i_T = 0.1 \text{ nM}$.

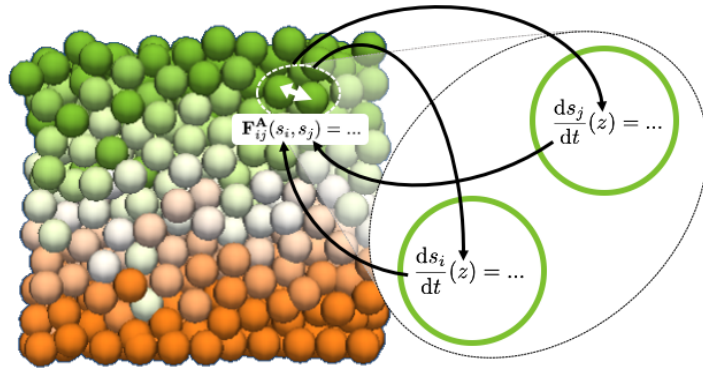


Fig 3. Diagram of the coupling between the multicellular and the subcellular scales. The cell gets its height from the multiscale model, updates the subcellular model parameters and solves for that time step, and then returns the updated proportion of remaining corneodesmosomes to the multicellular model to scale cell-cell adhesion.

Incorporation of subcellular model of adhesion into a multicellular model allows the study of desquamation

In order to build a full multiscale model of desquamation we couple the ODE system for subcellular desquamation with a multicellular model of the epidermis. Note, as we explain in the Model section, given the high proliferation rate used in the model, the rate parameters for the multicellular system are scaled in order to reduce the height of the system for computational efficiency. The cell's vertical location in the corneum, i.e. xi , in the multicellular system (acting as a proxy for pH) provides the input into the subcellular model. For each cell, at each multicellular timestep, the subcellular model is integrated over the duration of the multicellular model time step to give the updated adhesion (CND) proportion. The new proportion of CND is returned to the multicellular system, and is used to calculate the magnitude of the cell's adhesion to its neighbours. A diagram to illustrate this coupling is shown in Figure 3. A more detailed description of the multicellular model, including the coupling and desquamation model, is provided below in the Model section.

Using this multiscale model, we are able to produce a tissue that balances the rate of proliferation and desquamation to produce a healthy, homeostatic tissue. The

proportion of remaining corneodesmosome, s , for each cell is shown in an image of the simulation output in Figure 4a. In this figure we see that the adhesion level appears to degrade homogeneously as cells move up through the tissue. Secondly, the protein begins to visibly degrade after seven layers of cells, which is higher than the defined beginning of the corneum ($Z = 4$ CD), however we know from the subcellular model for a single cell that the initial degradation of s is slower (Figure 2). At the top of the tissue, cells detach in clumps, when the adhesion protein appears to have dropped to less than $s = 0.2$.

Figure 4c shows the mean thickness of the system over time and the estimated steady state thickness of the tissue and the corneum. We can see that this new system is able to maintain a steady state thickness. The steady state tissue and corneum thickness in Figure 4c is 14.8 CD and 10.8 CD respectively. We note there is a high variation in the height over time, which can also be seen in supplementary S1 Video. This is due to the definition of removed cells: they require a separation distance of 0.7 CD from the main tissue. This can be seen in Figure 4a, where the cells at the top of tissue are seen to be 2–3 CD from the layer below, but have still not been removed as there is a line of cells connecting to the tissue (note the system is periodic in the horizontal directions).

The values of the reactants over tissue thickness for one realisation, at $t = 30$ days, are shown in Figure 4b. The point data shows the multicellular simulation values, while the lines indicate the expected values using the single cell solution (determined using the mean velocity of the system). Note i is given as i_T/s_0 and therefore has a maximum value of 10^{-5} when $i_T = e_T = 0.1$ nM. This is shown in the inset in the figure. The results match the expected concentrations initially but then begin to diverge slightly towards the top of the tissue. This would be due to the higher cells experiencing effects from the removal force and therefore having an increased upwards velocity towards the top of the tissue. Figure 4b also shows little variation in the reactant concentrations in cells at any particular height—the mean range in s over 0.1 CD intervals in z is 3.0%—as we could see in Figure 4a.

Cells in the top layer of the tissue (those experiencing the removal force) had a median substrate level of $s = 0.18$. If we consider the system as a tetrahedron (i.e one cell being connected to 3 lower cells), this is close to what is expected to be required to break the 3 cell-cell bonds to the lower cell layer for removal. Given that the removal force is half the maximum adhesion force, it would be expected that s would need to drop to $s \approx 0.17$ for desquamation if the cell were separated from the three cells below at a separation distance equal to the peak of the adhesion curve. Note, however, in reality the cell configuration is highly random at the top of the tissue and, additionally, cells can ‘drag along’ cells below them when they are pulled from the top of the tissue, as seen in Figure 4a.

The final aspect of the healthy system we will discuss are the dynamics of cell turnover time and velocity, shown in Figure 4. Given a mean cell cycle time of 15 hours, and an expected layer thickness of 0.8 CD (for a tetrahedral packing), we would expect the velocity to be around 0.053 CDhr⁻¹. This is close to the calculated mean cell velocity, from the timeseries data shown in Figure 4d, which is found to be $v_z = 0.046$ CD.hr⁻¹. The mean velocity calculation excludes stem cells and cells at the top of the tissue, as their velocities are much higher than in the main tissue, and therefore their inclusion would bias the mean and not be representative of the main bulk of the tissue.

The cell turnover times are shown in Figure 4e. Again, we could make an estimate of what we expect the turnover times to be. Given a corneum thickness of 10.8 CD and a velocity of $v_z = 0.046$ CD.hr⁻¹, we would expect a corneum turnover time of around 235 hours. As can be seen in the plot, the median cell age at death is 290 hours, or 12.1 days. The median age of cells at entry to the corneum is 82 hours, this gives a

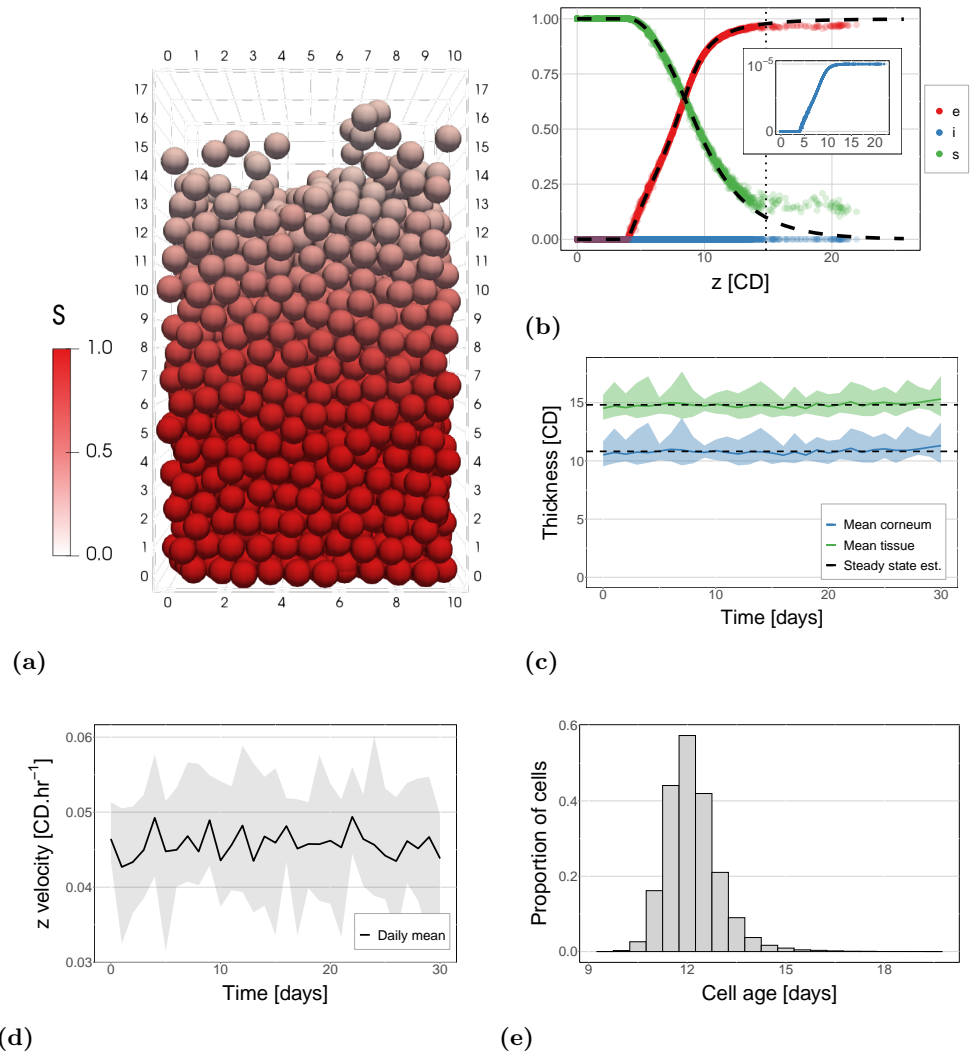


Fig 4. Healthy tissue model results. (a) An example of the simulation output for one time point. Cells are coloured by their proportion of remaining corneodesmosome (s). (b) Reactant levels for each cell at one time point in one simulation. The dashed black line shows the expected solution of the subcellular model given the expected vertical velocity. The inset shows the detail of the change in free inhibitor (LEKTI) levels. (c) The tissue thickness over time for all simulations. The dashed line shows the mean and the ribbon the minimum and maximum over time. Green indicates the overall tissue height and blue the corneum height (4 CD less than the tissue). (d) The average vertical velocity over time. The ribbon indicates the range seen across all simulations, and the line is the mean of the simulations. The velocity is calculated based on cells in the main tissue and does not include stem cells or cells that are experience the desquamation force. (e) The age at which cells are removed, also known as the turnover time.

turnover time in the corneum of 208 hours—lower than expected. However, as noted above, this velocity does not include cells experiencing the removal force. The average velocity of cells experiencing the removal force is $0.31 \text{ CD}\cdot\text{hr}^{-1}$, which would cause a decrease in the turnover time. Further reasons for this discrepancy are discussed in the results below for diseased tissue (decreased LEKTI).

Distinct proliferative cell niches can be represented by a homogeneous population

Experiments have shown evidence of two potential populations of proliferative cells exist in the basal layer with significantly different cell cycle lengths values [26–28]. We investigate the effect of two proliferative populations in our model by comparing different combinations of fast and slow cycling stem cell populations with the same harmonic mean: $H(T_C) = 12$ hours. The harmonic mean is used to account for the fact that the fast cycling cells will undergo more cycles than the slow cycling cells—it requires the proliferation rate across each setup to be the same. Due to this behaviour, we would expect an increased number of divisions to occur than would be inferred from the arithmetic mean. We also ran simulations using the same arithmetic mean (results not shown) which confirmed this.

To implement the two populations, we set 50% of the cells as fast cycling: $T_C = T_1$, and 50% as slow cycling: $T_C = T_1 + \Delta T_C$. We choose a range of values for ΔT_C and determine T_1 using the following equation:

$$T_1 = \frac{H_\mu - \Delta T_C}{2} + \frac{\sqrt{\Delta T_C^2 + H_\mu^2}}{2}, \quad (1)$$

where $H_\mu = 15$ hours is the desired value of the harmonic mean. The allocation of the fast or slow cycle length to the stem cells was random. The cell lineage used is: one stem cell produces one stem and one differentiated cell, making all stem cells in the system are immortal. Consequently, the ratio of fast to slow cells in the simulations persist at 50:50.

As can be seen in Figure 5, increasing the cycle difference but maintaining the same harmonic mean produces the same steady state thickness and mean velocities. This is because the harmonic mean accounts for the increased count of events occurring for cells with higher rates. If we calculate the average proliferation rate in each simulation it is found to be 1.60 divisions per day for each setup. Consequently, it is logical that the average velocity remains the same and, given we are not modifying any aspect of desquamation, therefore the thickness is also the same. Given this result, we know we can approximate the expected steady state thickness of a system with two populations of proliferative cells by a single population system with cycle time equal to the harmonic mean of the two populations.

Lower levels of LEKTI (inhibitor) cause premature desquamation

Netherton Syndrome (NS) is a disorder that mutates the gene for the LEKTI inhibitor, believed to reduce its concentration. Symptoms of NS include skin peeling, frequent skin infection, and temperature instability [13]. Presumably as a result of the reduced amount of inhibitor, KLK levels are elevated in NS patients. Komatsu et al. [13] recorded KLK levels in the NS patients between 157% to 486% that of healthy corneum. In order to simulate the effects of NS we can extend our model consider the effect of reduced LEKTI inhibitor on the tissue by reducing the concentration of the inhibitor, i_T .

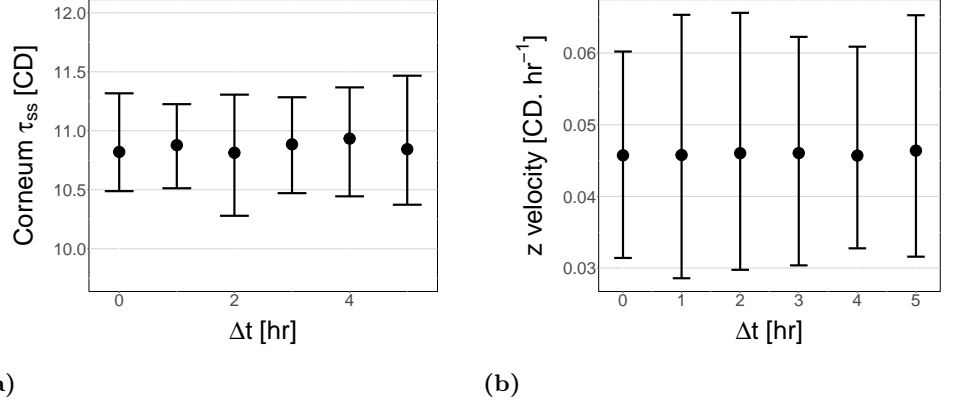


Fig 5. Results for simulations with two proliferative populations (two different cell cycle times). Δt is the difference in cycle time between the two populations, and the harmonic mean is the same for all configurations. In both plots the point shows the mean and the bars indicate the minimum and maximums across all simulations. (a) The steady state height of the corneum. Note that the mean is approximately the same regardless of the difference in cycle time between the two populations as they have the same harmonic mean. (b) The average velocity in the tissue (excluding stem and top cells). Again, this is approximately the same regardless of cell cycle difference due to each configuration having the same harmonic mean.

Figure 6a shows the simulation output for the system with no inhibitor present. Comparing this to Figure 4a shows no qualitative difference in the structure of the systems, except for the difference in thickness. Figure 6b show the mean thickness over time for different levels of inhibitor and the calculated steady states respectively. As would be expected, reducing the inhibitor reduces corneum thickness. This is because a reduced level of inhibitor causes increased amounts of enzyme available to degrade the adhesion proteins, resulting in earlier desquamation. We can see this in Figure 6c, where decreasing concentrations of inhibitor increases the amount of free enzyme e , and this increases the degradation rate of the adhesion protein s . We note that Figure 6c shows clearly the initial conditions for each inhibitor level at entry to the corneum: we assume all inhibitor (i) is in complex with the enzyme (e), and any remaining enzyme is free enzyme, as described later in the methods.

Figure 6b also shows that corneum thickness is linearly dependent on the concentration of inhibitor present in the system. When there is no inhibitor present the corneum thickness decreases by 28% (to 7.8 CD). The fitted line shown in Figure 6b is

$$\tau_{ss} = 7.78 + 3.05 \left(\frac{i_T}{e_T} \right). \quad (2)$$

However, in S2 File we show the use of an effective enzyme concentration decreases the effect of a reduction in inhibitor. Therefore, the reduction of 28% is expected to be a lower bound for the effect of the reduced inhibitor on tissue thickness.

We can also look at the change in the vertical velocity and turnover time. Changes to the inhibitor concentration should have no effect on the proliferation, and so we would not expect the velocity of the cells to change. This can be seen in Figure 7a, where there is negligible difference in mean velocity (relative range is 2.5%).

Figure 7b shows that the turnover time increases with the decreased inhibitor. This is to be expected as, given the same velocity, and increased height for the cell to traverse would cause an increase in migration time. This can be explored in more detail if we directly compare the turnover time and steady state corneum height, as seen in

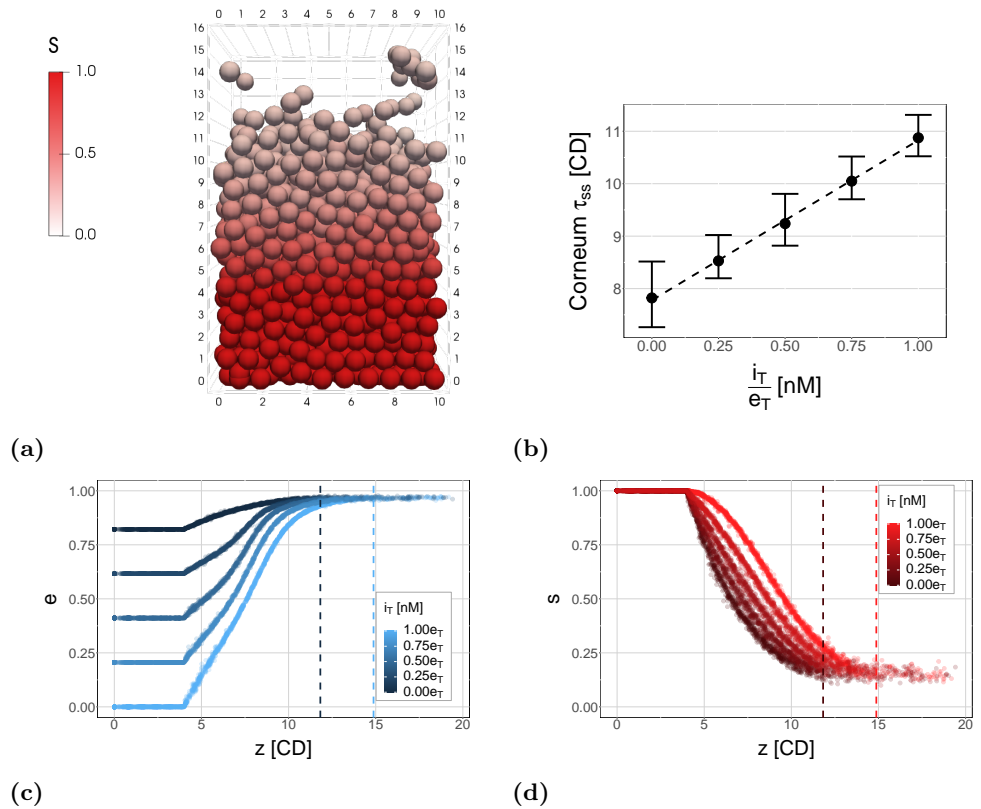


Fig 6. Tissue structure and thickness results for different amounts of inhibitor. (a) Simulation output from one simulation at one time point, showing the level of adhesion protein s in each cell. Note, there is no apparent difference in system dynamics compared to the healthy system, just an increased rate of reduced s in time and consequently seen in the vertical direction in the image. (b) The steady state thickness values. The dashed line is a linear fit to the points. (c) and (d) Diseased tissue s and e levels with different levels of inhibitor. The data is taken from the final time point of one simulation for each inhibitor concentration. The dashed lines show the steady state heights for $i_T = 0$ (black) and $i_T = e_T$ (blue or red).

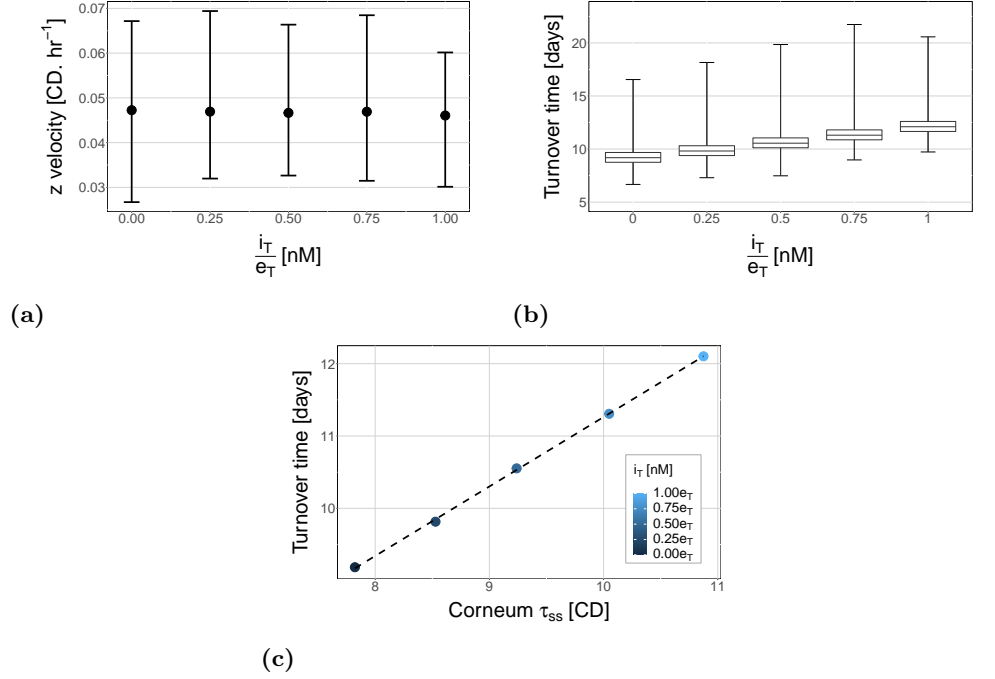


Fig 7. (a) The mean vertical cell velocity for different levels of inhibitor. (b) The cell turnover time, from birth to desquamation, for different levels of inhibitor. The box plot indicates the quartiles and mean, with the error bars showing the minimum and maximum. The box plot shows there are a large number of outlier cells with high turnover times. (c) The steady state against the cell turnover time. The dashed line is a linear fit to the points.

Figure 7c. The figure shows turnover time is proportional to corneum height, and the dashed line indicates the fit to the data:

$$T = 0.96\tau_{ss} + 1.66 \text{ [days]}. \quad (3)$$

We could expect the coefficient of τ_{ss} to be 0.91 days.CD⁻¹ given an average vertical velocity of $v_z = 0.046$ CD.hr⁻¹, and the constant to be 3.4 days, as this is the average age at entry to the corneum. There are three factors that are likely to contribute to this discrepancy. Firstly, the calculated turnover time is not identical to the average age at the determined tissue height. This is because tissue height is determined by the mean height of the top layer of cells, which would be lower than the mean height at which cells are lost (after they have sufficiently detached from the tissue), therefore increasing the coefficient and intercept to compensate. Secondly, the velocity is calculated using only ‘normal cells’: cells which are not stem or top of tissue cells. This is because the forces on the top cells (and the stem cells), are much stronger and therefore including these cells is not a good representation of the bulk tissue velocity. Consequently, the period of time in which cells are a top cell, and moving at higher velocities than the average, would be expected to reduce both the coefficient and the intercept. Thirdly, there are only 10 data points (simulations) for each steady state height calculated and so stochasticity in the system will have an effect.

Heterogeneous full recovery is more effective than homogeneous partial recovery

A multiscale multicellular model is well suited for investigating heterogeneous systems. If we consider the system above for diseased tissue, we could hypothesise that a treatment to restore the healthy system would be to increase the level of inhibitor in the cells. The efficacy of this hypothetical treatment can be seen above in Figure 6b where results show a linear relationship between the inhibitor concentration in the cells and the tissue thickness. However, one could also envisage a scenario in which such a treatment did not have 100% cell uptake, instead treating only a proportion of stem cells and leaving the remainder diseased. This is the scenario we investigate here.

We assume that the level of inhibitor in any cell is inherited from its parent stem cell and assign a level of inhibitor to each stem cell. The allocation of the diseased and healthy cells is random, so there is no spatial dependency. We set $i_T = 0$ for the diseased cells and $i_T = e_T$ for the healthy cells. Note there are 100 stem cells in the system. The proportion of healthy to diseased stem cells persists throughout the simulation given the cell lineage used (stem cell divides to create one stem and one differentiated daughter).

Figure 8a shows the thickness of the tissue with different counts of diseased cells. As can be seen in the figure, increasing the number of healthy stem cells has a non-linear effect on the corneum thickness. Here, we have fitted a quadratic curve to the thickness:

$$\tau_{ss} = 7.86 + 4.71p - 1.79p^2, \quad (4)$$

where p is the proportion of healthy cells. Consequently, in comparison to the results in Figure 6b, we can see that better outcomes are seen if only a proportion of cells recover full inhibitor concentration, compared to small increases to the concentration of inhibitor in all the cells.

Figure 8b shows the reactant levels of the cells at one time point in a simulation with half the stem cells diseased and the other half treated. As would be expected, half the cells (points) follow the diseased path and the other half the healthy path. Figures 8c and 8d are a simulation snapshot with cells coloured by the s and e levels. Supplementary materials S2 Video and S3 Video are videos of one simulation with cells coloured by s and e respectively. The diseased cells can be identified as the white cells when $z < 4$ CD in Figure 8c, and the healthy cells are blue. This shows their initial conditions which are assigned at birth, based on the proportion of i_T to e_T .

The plots and simulation snapshots in Figure 8 show that the diseased cells are not lost before the healthy ones, as might be expected given their increased adhesion degradation rate. As cells tend to be removed in clumps the diseased cells are held longer in the tissue, or in the clumps, by the healthy cells.

Finally, Figures 8e and 8f show the cell velocities and turnover times against height for each of the different proportions of healthy cells. Similar results are seen to the diseased system. Firstly, the mean velocity is similar between setups, as the proliferation rate is not changed. In this case it varies by 3.7%. Secondly, Figure 8f shows the same linear relationship between the steady state height and the median turnover time, again as expected given the velocity does not change. If we calculate the fit (as shown by the dashed line in the figure), we find that it is not exactly the same as Equation (3):

$$T = 0.98\tau_{ss} + 1.5 \text{ [days]}. \quad (5)$$

The slight variation in the coefficient and the constant is likely explained by stochasticity in the system.

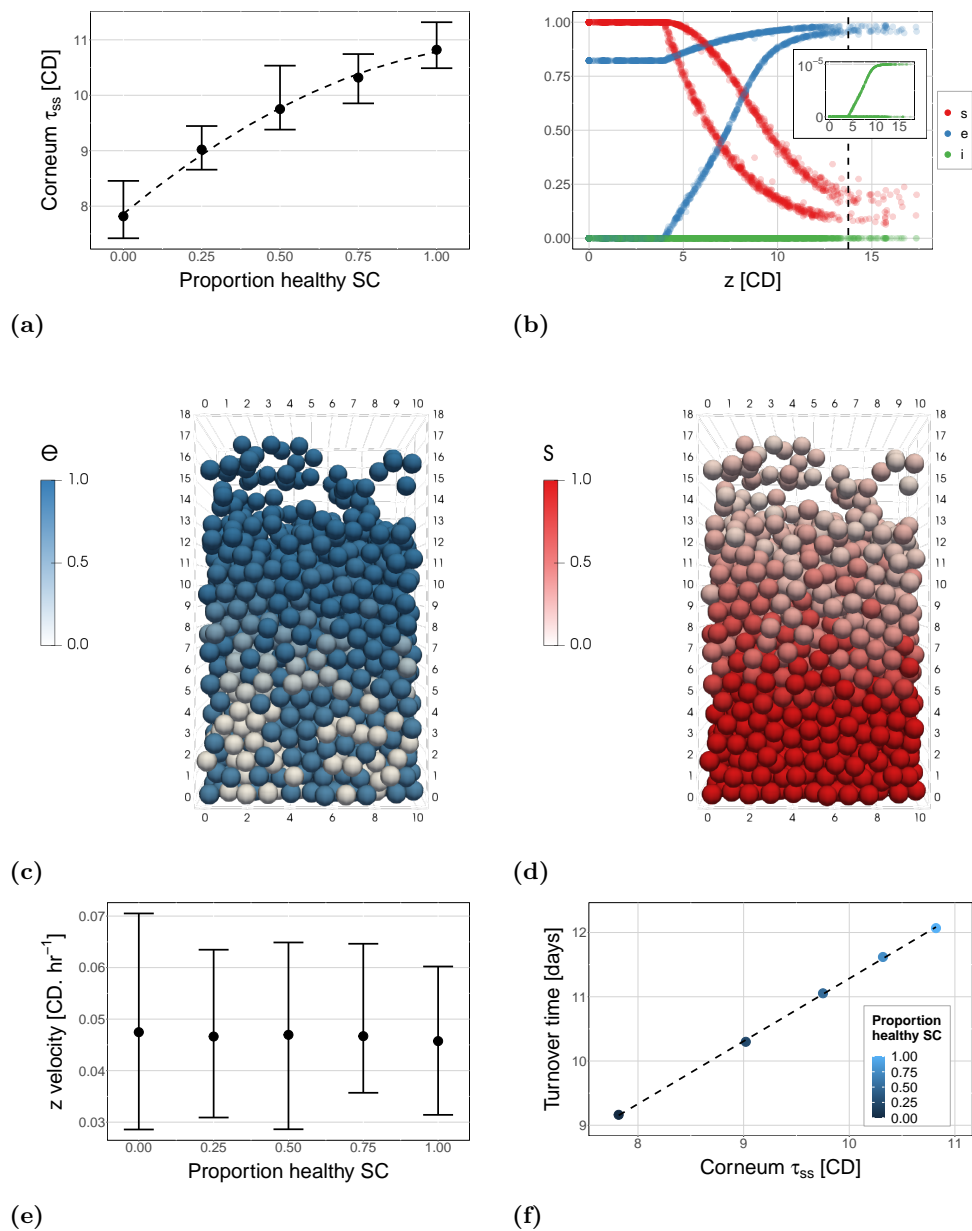


Fig 8. Hypothetical heterogeneous treatment simulation results. (a) Steady state corneum height for different proportions of healthy stem cells (producing cells with normal inhibitor levels, rather than diseased cells with no inhibitor). (b) The reactant levels of each cell for one time point where 50% of the stem cells produce cells with normal inhibitor level and 50% produce cells with no inhibitor. The dashed line is the steady state height. (c) and (d) Simulation output examples showing the cells coloured by their proportion of free enzyme, e (c) or proportion of remaining substrate, s (d). (e) The mean (points) and maximum/minimum (error bars) velocity of cells for the different proportions of healthy stem cells. (f) The median turnover times of differentiated cells against the steady state height for the different proportions.

Discussion

Emulating a homeostatic tissue

Our new subcellular model for desquamation supports the hypothesis of desquamation driven by KLK enzymes. In this hypothesis KLK enzymes degrade the corneodesmosomes (adhesion proteins) between the cells, a process which is inhibited by LEKTI and regulated by local pH. Though the results show that enzyme dynamics follow the expected function over pH, they also reveal there is a missing component to the model as the degradation occurs at too high a rate to match observed desquamation times *in vivo*. This missing component is likely to be a combination of the presence of the corneodesmosomes and other extracellular complexes limiting the diffusion of the enzymes, and therefore reducing the rate of degradation of the corneodesmosomes; and extrapolation of *in vitro* data to an *in vivo* environment.

In this paper we have introduced a multiscale model for desquamation of the epidermis. In Figure 4 we showed that this model is able to maintain a homeostatic tissue height. The height of the tissue is determined by the balance between the proliferation rate and the desquamation rate. The system with reduced LEKTI, in the case of diseased tissue, has an increased desquamation rate, changed this balance and hence the height of the tissue. Consequently, we can use such a multiscale system to investigate the effect of different aspects of proliferation and desquamation on tissue height.

Alternatively, from Figure 4b, we know all cells in the system follow a similar reduction in s , or adhesion proteins. Therefore it would be possible to approximate the decay with a sigmoidal (or equivalent) function. However, this would not provide the same level of information of the interaction between the subcellular and multicellular dynamics.

Insights into the system

We have used our multiscale model to investigate the effect of different epidermal attributes on tissue height and dynamics. The first attribute is the existence of two proliferative cell populations. Using the model we showed that the dynamics of a tissue with two proliferative populations can be approximated by a tissue with a single proliferative population. The proliferation rate of this single population is equal to the harmonic mean of the two proliferative populations.

The second investigation looked at diseased tissue: the genetic disease Netherton Syndrome, known to reduce production of the LEKTI inhibitor for the desquamation process. Our subcellular model results show that such a reduction in inhibitor is sufficient to explain the increased concentration of free enzyme observed in patient skin samples. Additionally, the multiscale model shows a decrease in the inhibitor has a noticeable effect on tissue thickness, though model approximations cause the system to underestimate the effect of the reduced inhibitor. The relationship between the inhibitor concentration and tissue thickness is also shown to be linear. If we considered a hypothetical treatment for the diseased cells, that only cures a proportion of the proliferative cells, tissue thickness increases approximately quadratically with the number of cells treated. Consequently, full cure of a proportion of proliferative cells is shown to be slightly better than partial cure of all proliferative cells.

Limitations and future work

Several simplifications are always necessary in order to produce a computationally efficient system. In addition, there are likely a multitude of processes occurring at both a

subcellular and multicellular level that are unknown and affect the processes described by this model.

With respect to the subcellular model, one known limitation is not explicitly accounting for the structure of the extracellular space in degradation of the adhesion structures. As discussed in the results, it is possible that the adhesion structures we consider here (corneodesmosomes) are limiting the diffusion of the enzyme, as well as other structures, such as tight junctions, which are not included in the model [8]. Future work could look in more detail at the potential affect of limited diffusion on the degradation rate. However, this study would currently be limited by a lack of data for parameterisation.

Related to this, the parameterisation of the subcellular model is built around data that is often unable to be recorded *in vivo*. Consequently, it has been necessary to extrapolate much of the data from a laboratory setting to a physiological settings. This applies to both the rate parameters and reactant concentrations. Such an extrapolation requires many assumptions which are unable to be tested. Consequently, as potential improved testing methodologies, or more comprehensive data, become available it will be possible to improve this model.

Another area that is affected by a lack of data is the force experienced by the cells to enable desquamation. It is difficult to understand the forces applied to the skin in everyday life, both in type (i.e. shear or tension) and magnitude. However, given we currently ignore any anisotropy in the distribution and degradation of the adhesion molecules, and additionally do not know the strength of the adhesion molecules between cells, this level of detail is not required. We are interested in investigating the anisotropy of degradation in future work. We expect such a study would be strongly linked to the proposed study above on the structure of the extracellular space and limited diffusion.

Two further simplifications of the multicellular model are the use of spherical, rather than ellipsoidal cells, and a flat basal membrane. In the stratum corneum, cells are almost flat disks with a diameter of 20–40 μm , and a height of less than 0.5 μm [30–32]. The use of spherical cells will clearly influence these results, as the packing of the cells will change depending on cell shape. This would likely scale the determined function linking subcellular parameters and tissue height, however we would not expect it to change the shape of these functions and hence the discussed insights from these results. With the use of an undulating rather than a flat membrane, we would expect much more variation in the results with respect to turnover time and velocities, however again qualitatively the results would not change.

Model

In this section we detail the implementation of our multiscale model. First, we describe the development of the subcellular model for adhesion degradation, including the ODE system, parameterisation, and initial conditions. Then we briefly present the base multicellular model, and the coupling between the subcellular and multicellular models. Finally, we detail how we implement force based desquamation in the multiscale model.

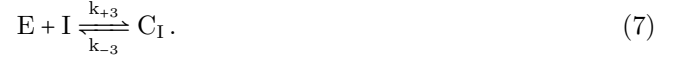
A subcellular system

We are interested in developing a subcellular model of the adhesion degradation over time for the process shown in Figure 1. This model takes a spatial pH gradient as an input, and then models the interaction between LEKTI, KLKs, and corneodesmosomes for each cell individually using mass action kinetics. The rate parameters depend on the changing pH as the cell moves up through the tissue and experiences the pH gradient.

The output of this model is the proportion of adhesion molecules (CND) remaining for each cell, which scales the cell-cell adhesive force of the multicellular model.

Subcellular differential equations

We convert the system described in Figure 1 into the competitive inhibition chemical equations:



where E is the KLK enzymes, S is corneodesmosome adhesion proteins, I is the inhibitor LEKTI, P is the product(s) corneodesmosome degradation produces, C_S is the complex formed between the KLKs and the corneodesmosome, and C_I is the complex formed between the KLKs and LEKTI. All rate parameters, k_{+1} , k_{-1} , k_2 , k_{+3} , and k_{-3} , are initially assumed to be functions of local pH.

We take this system of chemical equations and produce a set of ODEs using mass action kinetics. In order to simplify the computation and analysis, we scale the system by the enzyme and corneodesmosome concentrations. We define the following dimensionless variables: $s = [S]/s_0$, $i = [I]/s_0$, $p = [P]/s_0$, $e = [E]/e_T$, $c_s = [C_S]/e_T$, and $c_i = [C_I]/e_T$, where $[X]$ is the concentration of species X in Equations (6) and (7); s_0 is the initial concentration of adhesion proteins; and $e_T = [E] + [C_S] + [C_I]$ is the total enzyme present, which is conserved. This gives the following system of equations:

$$\frac{de}{dt} = -k_{+1}s_0es + (k_{-1} + k_2)c_s - k_{+3}s_0ei + k_{-3}c_i, \quad (8)$$

$$\frac{ds}{dt} = -k_{+1}e_Tes + k_{-1}\frac{e_T}{s_0}c_s, \quad (9)$$

$$\frac{di}{dt} = -k_{+3}e_Tei + k_{-3}\frac{e_T}{s_0}c_i, \quad (10)$$

$$\frac{dc_s}{dt} = k_{+1}s_0es - (k_{-1} + k_2)c_s, \quad (11)$$

$$\frac{dc_i}{dt} = k_{+3}s_0ei - k_{-3}c_i, \quad (12)$$

$$\frac{dp}{dt} = k_2\frac{e_T}{s_0}c_s. \quad (13)$$

pH gradient

The local pH is the input for the ODE system for the cell, and depends on cell location. The pH gradient was fit to data obtained from a graph in Ohman et al. [14] for pH in human forearm, abdomen, and calf epidermis collected using sello-tape. The function fit for the pH gradient, with an R-squared of $R^2 = 0.94$, is as follows:

$$\text{pH} = f_{\text{pH}}(\xi) = 6.8482 - 0.3765\xi - 5.1663\xi^2 + 3.1792\xi^3, \quad (14)$$

where $\xi \in [0, 1]$ is the height of the cell above the base of the corneum as a proportion of the corneum thickness.

Rate parameters for the subcellular system alone

Equations (8) to (13) require five rate parameters: three for the interaction between the enzyme and the corneodesmosomes; k_{+1} , k_{-1} , and k_2 , and two for the interaction

between the enzyme and LEKTI inhibitor; k_3 and k_{-3} . We can estimate values for these parameters, the pH gradient, and the reactant concentrations using data from the literature. The parameters determined here are for the subcellular model results. These parameters are modified for the multiscale model implementation, which is discussed in the The multiscale model section. We provide a summary here, for more details see S1 File.

The rate parameters for the LEKTI-KLK (inhibitor-enzyme) reaction, Chemical Equation (7), are determined from *in vitro* experiments by Deraison et al. [5]. This study determined association and dissociation rates between LEKTI and KLK molecules at 4 different pH values. Fitting models to this data produces the following equations for k_{+3} and k_{-3} as functions of pH:

$$k_{+3} = f_{+3}(\text{pH}) = (5.2 \text{ pH} - 19.5) \times 10^7 [\text{M}^{-1} \cdot \text{hr}^{-1}], \quad (15)$$

$$k_{-3} = f_{-3}(\text{pH}) = 2.3 \times 10^6 e^{-3.0\text{pH}} [\text{hr}^{-1}], \quad (16)$$

with R-squared values of $R^2 = 0.94$ and $R^2 = 0.9998$ respectively.

The data used to parameterise the corneodesmosome-KLK (adhesion-enzyme) interaction, Chemical Equation (6), is from Caubet et al. [10]. This study recorded the degradation of two corneodesmosome proteins incubated with KLK5 in both neutral (pH= 5.6) and acidic (pH= 7.2) pH over a two hour incubation period. However, as the authors point out, there appears to be little variation between the two in the data. Additionally, this data set is small and so it is not reliable to calculate fits with high confidence considering the different pH levels separately. Consequently, for this reaction we assume the effect of pH is negligible.

In order to determine the parameters to the data from Caubet et al. [10], it is necessary to simplify the system. Given the experiments were performed without inhibition, we can reduce our set of equations in Equations (8) to (13) and apply the quasi-steady state assumption of Briggs et al. [33]. This gives a relationship between remaining protein, s , and time which can be solved to determine k_2 and the Michaelis constant, K_M :

$$K_M = \frac{k_{-1} + k_2}{k_{+1}}. \quad (17)$$

A full description of the relationship was determined and the fits is given in S1 File. The calculated values are shown in Table 1.

Parameter		Value: multiscale	Value: single cell
KLK-CND Michaelis constant	K_M	$4.60 \times 10^{-5} \text{ M}$	$4.60 \times 10^{-5} \text{ M}$
C_S degradation rate	k_2	$6.87 \times 10^3 \text{ hr}^{-1}$	$2.29 \times 10^3 \text{ hr}^{-1}$
KLK-CND association rate	k_{+1}	$1.49 \times 10^8 \text{ M}^{-1} \cdot \text{hr}^{-1}$	$4.97 \times 10^7 \text{ M}^{-1} \cdot \text{hr}^{-1}$
Repulsive spring constant	k	$150 \mu\text{N}$ [34]	
Adhesion force shape parameter	γ	7 [25]	
Adhesion force coefficient	α	$374.7 \mu\text{N}$	
Cell cycle time	T_C	$\sim U(13, 17)$	

Table 1. The parameter values for the subcellular and multiscale model. Values are given for the multiscale model and the rate parameters used for the single cell system are given in parentheses.

From the Michaelis constant, K_M , it is necessary to determine the values of k_{+1} and k_{-1} in order to solve the system. Given K_M is on the order of 10^{-5} and k_2 on the order of 10^3 , k_{+1} is approximately five to eight orders of magnitude greater than k_{-1} (from Equation (17)). Consequently, we assume that the value of k_{-1} is negligible and we approximate $k_{-1} = 0$. Solving the full ODE system for different values of k_{-1} at both

acidic and neutral pH supports this assumption—the change in $s(T)$ is less than 0.01% at either pH for $k_{-1} \in [0, 10^4]$. Consequently, we get the value for k_{+1} shown in Table 1.

Concentrations of reactants

There is limited *in vivo* data for the concentrations of KLK, LEKTI, and CNL in the corneum. Most data in the literature is not available as concentrations, as is required for the model, and hence has to be approximated. Consequently, these values are very rough estimations, and only provide an idea of the order of magnitude of the relative concentrations of the reactants. A summary of how the concentrations were determined is given below, with more detail in the S1 File.

Several studies have investigated the weight of KLK in epidermal tissue. The data is commonly provided as a weight of free enzyme per weight of dry corneum tissue. Consequently, it does not account for enzyme in complex and provides no spatial component to the concentrations. It is necessary, for the purposes of the model, to convert these amounts to molar concentrations in extracellular space. This was done using an approximate molecular weight of KLK5, the water content of the corneum, and the volume ratio of cell to extracellular space in the corneum. Values for all of these parameters are given in Table 2.

Parameter	Value	Reference
Dry weight of KLK5 enzyme	3.1 ng.(mg dry tissue ⁻¹)	[13]
Molecular weight of KLK5	33 kDa	[12]
Water content of corneum	0.5 g.g ⁻¹	[35]
Volume proportion of extracellular water	13%	[30, 36]
Estimated enzyme concentration	0.723 μM	

Table 2. Parameters used to determine the concentration of KLK5 enzyme.

The second reactant is the inhibitor LEKTI. A study by Fortugno et al. [12] determined LEKTI fragments most effective at inhibiting KLK5 were present in the same molar quantities as KLK5. Consequently, we set $i_T = e_T$ in healthy epidermis.

The final reactant is the corneodesmosome, or adhesion proteins. The *in vivo* data on corneodesmosomes provides counts of associated proteins across the edges of cells. In order to convert this into a concentration we need to determine the number of proteins per unit of extracellular volume. This requires information on the cell size and the ratio of cells to extracellular space. This is given in the Table 3. We note the corneodesmosome proteins concentration is only one order of magnitude greater than the enzyme concentration.

Parameter	Value	Reference
Protein count on peripheral of cell	16 μm^{-1}	[8]
Protein count on central region of cell	10 μm^{-1}	[8]
Dimensions of cell (width \times height)	30 \times 0.3 μm	[30]
Extracellular space between cells	0.044 μm	[36]
Estimated corneodesmosome protein concentration	6.6 μM	

Table 3. Parameters used to determine the concentration of corneodesmosome proteins.

Initial conditions

The initial conditions for the subcellular model are the concentrations of the reactants upon entry to the corneum (assigned at birth). Corneodesmosomes are at their

maximum concentration initially ($s(t=0) = 1$) as the cells have the maximum adhesion at the start of the corneum. We assume the enzyme and inhibitor start in complex (c_i), limited by whichever of the enzyme or inhibitor has a lower concentration. If there is more enzyme than inhibitor, we could assume that the remaining enzyme is free, i.e. $c_s(t=0) = 0$, however this is a stiff system and the solution therefore requires very small time steps to solve and has the potential to cause numerical issues (can be seen in supplementary material S2 File). Consequently, we instead assume that any enzyme that is not complex with the inhibitor is in an instantaneous quasi-equilibrium with the substrate-enzyme complex.

In order to calculate what the equilibrium state would be we first assume all inhibitor is in complex with the enzyme. For the remaining enzyme, we assume the enzyme-substrate reaction, Equation (8), is approximately equal to zero. Given we are estimating the dynamics instantaneously upon the release of these reactants, we set $s = 1$. This gives the following relationship between e and c_s :

$$-k_{+1}s_0e + (k_{-1} + k_2)c_s = 0. \quad (18)$$

We know $k_{-1} = 0$ and, additionally, due to conservation of the enzyme $e + c_s + c_i = 1$. Therefore the initial conditions become:

$$e(t=0) = e^* = \frac{k_2}{k_{+1}s_0 + k_2} \left(1 - \frac{i_T}{e_T}\right), \quad (19)$$

$$c_s(t=0) = 1 - e^* - \frac{i_t}{e_t}, \quad (20)$$

$$c_i(t=0) = \frac{i_T}{e_T}, \quad (21)$$

with $s(t=0) = 1$ and $i(t=0) = 0$. Parameters i_T and e_T are the concentration of inhibitor and enzyme respectively, with $i_T \leq e_T$.

The multiscale model

In order to build the multiscale model we incorporate the ODE system described in Equations (8) to (13) into our multicellular model. This DE system regulates the degradation of adhesion for each cell in order, such that it can undergo the desquamation process. In order to efficiently incorporate the subcellular model described above we scale the rate parameters to suit the multicellular model parameters and speed up computation. In order to effectively model the desquamation process using adhesion degradation, we also incorporate a removal force into the multicellular model so that we can determine the cells to remove from the tissue. This is described below.

Base multicellular model

We use a modified version of the multicellular model in [24]. This model uses an overlapping spheres methodology, where cells interact with each other via adhesion and repulsion forces, and with the basal membrane. Cell movement is determined from the inertia-less force balance:

$$\eta \frac{d\mathbf{c}_i}{dt} = \sum_{j \in N_i} \mathbf{F}_{ij} + \mathbf{F}^{\text{Rt}} + \mathbf{F}^{\text{D}}, \quad (22)$$

where \mathbf{c}_i is the cell centre location of cell i ; N_i is the set of neighbours of cell i ; \mathbf{F}_{ij} are the forces on cell i due to interacting neighbour cell j ; $\mathbf{F}_{i,\text{ext}}$ are any external forces acting on cell i ; and η is the viscous drag coefficient for the cell [37]. \mathbf{F}^{Rt} is a rotational force applied during division in order to maintain the stem cells in the basal layer, as

described in detail in [24]. \mathbf{F}^D is the desquamation force, shown in Figure 9 and described in a later section.

We define the cell-cell spring vector $\mathbf{s}_{ij} = s_{ij}\mathbf{n}_{ij}$, for $s_{ij} = \|\mathbf{c}_j - \mathbf{c}_i\| - r_{ij}$ where r_{ij} is the sum of the cell radii for cells i and j , and \mathbf{n}_{ij} is the unit vector between the two cells. The adhesion and repulsion forces are then defined to be:

$$\mathbf{F}_{ij} = \begin{cases} -\alpha \left((s_{ij}^* + c) e^{-\gamma(s_{ij}^* + c)^2} - c e^{-\gamma(s_{ij}^{*2} + c^2)} \right) \mathbf{n}_{ij}, & s_{ij} > 0, \\ 0, & s_{ij} = 0, \\ k \log(1 + s_{ij}) \mathbf{n}_{ij}, & s_{ij} < 0, \end{cases} \quad (23)$$

$$\text{where } c = \sqrt{\frac{1}{2\gamma}}, \quad (24)$$

$$\text{and } s_{ij}^* = \frac{s_{ij}}{r}, \quad (25)$$

where k is the repulsive spring constant [25, 38], and α is the adhesion coefficient [25]. The values of the parameters are all shown in Table 1. Note, the adhesion coefficient for two cells not in the corneum is much higher than that used in previous papers [24, 25] ($374.7 \mu\text{N}$ rather than $0.2 \mu\text{N}$), due to the removal forces applied to the system, as described below. The value of α for any particular cell pair in the corneum is determined by the subcellular model, also described below.

Additionally, as in [24], we first simulate a fill period during which height restrictions are placed on stem cells in the basal layer, and cells are removed based on their height, rather than using the desquamation model. This is to establish the tissue, as we are interested in homeostasis rather than development. However, given we must define a sloughing thickness during this fill period, the thickness at the end of the fill period is not the steady state thickness of the system. Therefore, in order to ensure we are at steady state thickness, we also run the system for a burn-in period until it has reached a quasi-steady state, which is determined visually. Results are shown for 30 days of simulation, and therefore we set the minimum burn-in time to also be 30 days, giving a total simulated period of at least 60 days. We found, by visual inspection, that this is more than sufficient in all cases for the system to reach a steady state thickness. We only show the results for the final 30 days, and this is the period we use to calculate the steady state.

Due to stochasticity in the proliferation cycle, 10 realisations are run for each simulation setup. The horizontal boundaries are periodic, the base is bounded by the basal membrane, and the top boundary is defined by the desquamation process explained below. Further mechanisms are added to this model in order to model desquamation, and these are described in a later section.

Rate parameter modifications for the multiscale model

In order to produce a more computationally efficient system we decrease the number of cell layers in the tissue and use a high proliferation rate. We note, increasing the proliferation rate is simply a scaling of the system in time. Therefore the subcellular rate parameters (k_{+1} , k_2 , k_{+3} , and k_{-3}) need to be adjusted to account for this. The fit for pH in Equation (14) is already normalised to the thickness of the stratum corneum and therefore this does not need to be changed.

For the subcellular system alone we estimated the cell migration time as 20 days (480 hours) across the corneum. In multiscale system we have a much shorter migration time, due to the increased proliferation and desired decreased tissue thickness. From previous results [24], we know that the upwards velocity of the cells in the multicellular system is approximately $v_z = 0.05 \text{ CD}\cdot\text{hr}^{-1}$. This gives a migration time of 160 hours for

a target corneum thickness of 8 CD (cell diameters). Consequently, to change from a transit time of 20 days to 160 hours, we scale all rate parameters by 3. This gives the rate parameters for the enzyme-substrate reaction shown in Table 1, and the following equations for the enzyme-inhibitor reaction:

$$k_{+3} = g_{+3}(\text{pH}) = (15.6\text{pH} - 58.5) \times 10^7 [\text{M}^{-1} \cdot \text{hr}^{-1}], \quad (26)$$

$$k_{-3} = g_{-3}(\text{pH}) = 6.9 \times 10^6 e^{-3.0\text{pH}} [\text{hr}^{-1}]. \quad (27)$$

Combining the multicellular and subcellular model

The coupling and solution of the ODE model follows Algorithm 1. The subcellular degradation model is solved for each cell in the system for each time step. The only exclusion is the first few layers, where $z < h$ for some specified h (here $h = 4$), of cells, which are assumed to be in the lower layers of the epidermis, where we set the ODE system to zero. Both the cell location and current tissue height are taken from the multicellular model to determine pH, and consequently the rate parameters. Note, we only update the tissue height at every output time step due to the high stochasticity in the height of the system, as seen in the Results section. A comparison to results in which the height is recalculated at every time step (results not shown) show minimal difference in the determined height. The output from the cell into the multicellular system is the current proportion of s , or adhesion proteins, remaining. We ignore any anisotropy in adhesion degradation around the cell, as the driving forces we use to mimic the desquamation process are implemented in the vertical direction only.

The multicellular model then needs to relate the proportion of adhesion proteins to the cell-cell adhesion function. The proportional loss of the proteins is assumed to be directly proportional to the loss of adhesion, as these proteins provide the cell-cell adhesion. In order to determine the adhesion between two cells we use the mean of the two protein concentrations.

Modelling desquamation in the multiscale model

In order to model desquamation using the degradation of adhesion as the mechanism, we implement force-based cell removal. In force-based cell removal, a force is applied to the top cells in the tissue, which causes them to separate from the main tissue body. A similar force has previously been used by Li et al [25]. Once a cell, or a set of cells, is completely separated from the main tissue body, it is removed from the simulation. This method can be broken down into three mechanisms: the definition of top of tissue cells; the removal force; and the definition of separated cells. We address each of the three mechanisms individually below, and also show a two dimensional example of the method in Figure 9.

Defining the top cells

First, we need to determine which cells are at the top of the tissue. We do this by splitting the horizontal plane into a square grid with grid size Δx . We loop over the cell population and determine the highest cell (using the cell centres) in each grid square. This cell is labelled as a ‘top cell’.

Intuitively, one would calculate the density of each cell layer to determine an appropriate value of Δx . However, the simulation output does not show clear layering, and therefore it is difficult to determine a cell density. Close to the basal layer, where more layering is present, cell densities are around 1.2 cells/CD² (CD: cell diameters). However, after about the fourth layer, the cell arrangement is no longer obviously layered, becoming increasingly random, and cell density starts to decrease.

Algorithm 1: Linking the subcellular model to cell-cell adhesion in the multicellular model

for *each multicellular model time step* **do**

for *every cell* **do**

 Determine the parameters:

1. Height in corneum given cell location (z) and current corneum thickness (τ), $\xi = \frac{z}{\tau}$,
2. $\text{pH} = f_{\text{pH}}(\xi)$ using Equation (14),
3. $k_{+3} = g_{+3}(\text{pH})$ and $k_{-3} = g_{-3}(\text{pH})$ using Equations (26) and (27),
4. k_{+1} and k_2 from Table 1.

 Solve Equations (8) to (13) using CVODE to next time step,

 Store s for the cell.

end

for *every cell pair* **do**

 Get s_i and s_j for the two interacting cells i and j ,

 Calculate interaction force (Equation (23)), with scaled adhesion coefficient:

$$\alpha_{ij} = \frac{1}{2}(s_i + s_j)\alpha_0, \quad (28)$$

 where α_{ij} is the adhesion coefficient between cells i and j , and α_0 is the normal cell-cell adhesion coefficient.

end

for *every cell* **do**

 Calculate the rotational force if applicable,

 Add the desquamation force if top cell,

 Determine new cell location using Equation (22).

end

 Check if any cells have detached from the tissue and remove.

 Determine new set of cells that form the top layer of the tissue.

end

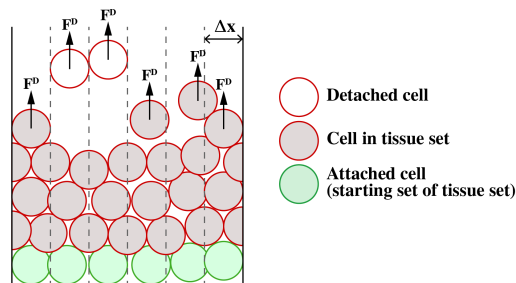


Fig 9. The desquamation model. Top cells experience a vertical desquamation force. Once they detach from the tissue they get removed. Detachment is defined by determining the connected tissue set, starting with the set of attached cells.

Consequently, for simplicity and symmetry with proliferating cell count we use a grid size of $\Delta x = 1$ CD. This means 100 cells are undergoing desquamation at any point in time, equal to the number of proliferating cells. Changing this grid density does not qualitatively change the results.

Removal force

Once we have identified which cells are the top cells we can then apply the removal force, \mathbf{F}^D in Equation (22), as shown in Figure 9. The removal force is of set magnitude and is intended to reflect the environmental forces experienced by exposed skin cells. Though we would not expect the forces to be vertical in reality, we neglect any horizontal shear forces for the purposes of our model. What is important is that the bonds between cells are sufficiently broken to allow removal. The reduction in cell-cell adhesion is due to the degradation of the cell-cell bonds, which is known to occur earlier in the vertical direction than the horizontal direction [8]. Consequently, we believe a vertical force is a good approximation of this process.

Detached cells

Once the force is applied to the top cells, they start to separate from the tissue and we need to define when cells are no longer connected to the main tissue body. We do this by determining the cell set that constitutes the main tissue body. Starting with a set of cells which we know are in the main body, we can determine which cells are in contact with this set of cells. We iteratively add the contacting cells to the set, and repeat this process until no new cells are added to the set. This is then our main tissue body, and any cells not in the set are considered separated, and consequently removed. We use the set of cells attached to the basal membrane as our initial set.

In order for prompt removal of the cells, such that the removal process has minimal effect on the tissue thickness, we use a removal, or desquamation, force of $\mathbf{F}_D = 5 \mu\text{N}$. In the presence of no other forces, a cell experiencing this force would be removed from the tissue in 1.4 hours (12% of the cell cycle). However, as a result of using this increased force for removal, an increased adhesion force is required to counter the effects of this force until the adhesion is sufficiently degraded. For simplicity, we set our adhesion force to twice that of the removal force: $\max(\mathbf{F}_{ij}(s_{ij} \geq 0)) = 10 \mu\text{N}$. We note that this is not the same as setting $\alpha = 10 \mu\text{N}$ in the adhesive function in Equation (23)—the equivalent coefficient value is $\alpha = 374.7 \mu\text{N}$. Changing this relationship between the expected removal forces and cell-cell adhesion force coefficient would change the point at which the removal occurs during the degradation function, however this would not qualitatively change the results.

Chaste implementation

The full multiscale model is implemented using the Chaste simulation libraries [39–41] for cardiac and multicellular tissue simulations. Chaste is a C++ library and the core code can be found at <https://chaste.cs.ox.ac.uk/trac/wiki>. To reproduce the model and results in this paper, further code and documentation can be found at <https://github.com/clairemiller/MultiscaleModellingDesquamationInIFE>.

Acknowledgements

This research was supported by an Australian Government Research Training Program (RTP) Scholarship, and in part conducted and funded by the Australian Research Council Centre of Excellence in Convergent Bio-Nano Science and Technology (project number CE140100036).

References

1. Cursons J, Gao J, Hurley DG, Print CG, Dunbar PR, Jacobs MD, et al. Regulation of ERK-MAPK Signaling in Human Epidermis. *BMC Systems Biology*. 2015;9:41. doi:10.1186/s12918-015-0187-6.
2. Evans ND, Oreffo ROC, Healy E, Thurner PJ, Man YH. Epithelial Mechanobiology, Skin Wound Healing, and the Stem Cell Niche. *Journal of the Mechanical Behavior of Biomedical Materials*. 2013;28:397–409. doi:10.1016/j.jmbbm.2013.04.023.
3. Menon GK, Cleary GW, Lane ME. The Structure and Function of the Stratum Corneum. *International Journal of Pharmaceutics*. 2012;435(1):3–9. doi:10.1016/j.ijpharm.2012.06.005.
4. Egawa G, Kabashima K. Barrier Dysfunction in the Skin Allergy. *Allergology International*. 2018;67(1):3–11. doi:10.1016/j.alit.2017.10.002.
5. Deraison C, Bonnard C, Lopez F, Besson C, Robinson R, Jayakumar A, et al. LEKTI Fragments Specifically Inhibit KLK5, KLK7, and KLK14 and Control Desquamation through a pH-Dependent Interaction. *Molecular Biology of the Cell*. 2007;18(9):3607–3619. doi:10.1091/mbc.e07-02-0124.
6. Ishida-Yamamoto A, Igawa S. The Biology and Regulation of Corneodesmosomes. *Cell and Tissue Research*. 2015;360(3):477–482. doi:10.1007/s00441-014-2037-z.
7. Matsui T, Amagai M. Dissecting the Formation, Structure and Barrier Function of the Stratum Corneum. *International Immunology*. 2015;27(6):269–280. doi:10.1093/intimm/dxv013.
8. Igawa S, Kishibe M, Murakami M, Honma M, Takahashi H, Iizuka H, et al. Tight Junctions in the Stratum Corneum Explain Spatial Differences in Corneodesmosome Degradation. *Experimental Dermatology*. 2011;20(1):53–57. doi:10.1111/j.1600-0625.2010.01170.x.
9. Borgoño CA, Michael IP, Komatsu N, Jayakumar A, Kapadia R, Clayman GL, et al. A Potential Role for Multiple Tissue Kallikrein Serine Proteases in Epidermal Desquamation. *Journal of Biological Chemistry*. 2007;282(6):3640–3652. doi:10.1074/jbc.M607567200.

10. Caubet C, Jonca N, Brattsand M, Guerrin M, Bernard D, Schmidt R, et al. Degradation of Corneodesmosome Proteins by Two Serine Proteases of the Kallikrein Family, SCTE/KLK5/hK5 and SCCE/KLK7/hK7. *Journal of Investigative Dermatology*. 2004;122(5):1235–1244. doi:10.1111/j.0022-202X.2004.22512.x.
11. Ishida-Yamamoto A, Deraison C, Bonnart C, Bitoun E, Robinson R, O'Brien TJ, et al. LEKTI Is Localized in Lamellar Granules, Separated from KLK5 and KLK7, and Is Secreted in the Extracellular Spaces of the Superficial Stratum Granulosum. *Journal of Investigative Dermatology*. 2005;124(2):360–366. doi:10.1111/j.0022-202X.2004.23583.x.
12. Fortugno P, Bresciani A, Paolini C, Pazzagli C, El Hachem M, D'Alessio M, et al. Proteolytic Activation Cascade of the Netherton Syndrome–Defective Protein, LEKTI, in the Epidermis: Implications for Skin Homeostasis. *Journal of Investigative Dermatology*. 2011;131(11):2223–2232. doi:10.1038/jid.2011.174.
13. Komatsu N, Saijoh K, Jayakumar A, Clayman GL, Tohyama M, Suga Y, et al. Correlation between SPINK5 Gene Mutations and Clinical Manifestations in Netherton Syndrome Patients. *Journal of Investigative Dermatology*. 2008;128(5):1148–1159. doi:10.1038/sj.jid.5701153.
14. Ohman H, Vahlquist A. In Vivo Studies Concerning a pH Gradient in Human Stratum Corneum and Upper Epidermis. *Acta Dermato-Venereologica*. 1994;74:375–379. doi:10.2340/0001555574375379.
15. Stekel D, Rashbass J, Williams ED. A Computer Graphic Simulation of Squamous Epithelium. *Journal of Theoretical Biology*. 1995;175(3):283–293. doi:10.1016/S0022-5193(95)80011-5.
16. Romijn LB, Almet AA, Tan CW, Osborne JM. Modelling the effect of subcellular mutations on the migration of cells in the colorectal crypt. *BMC Bioinformatics*. 2020;21(1):95. doi:10.1186/s12859-020-3391-3.
17. Sun T, Adra S, Smallwood R, Holcombe M, MacNeil S. Exploring Hypotheses of the Actions of TGF-*B1* in Epidermal Wound Healing Using a 3D Computational Multiscale Model of the Human Epidermis. *PLOS ONE*. 2009;4(12):e8515. doi:10.1371/journal.pone.0008515.
18. Adra S, Sun T, MacNeil S, Holcombe M, Smallwood R. Development of a Three Dimensional Multiscale Computational Model of the Human Epidermis. *PLoS ONE*. 2010;5(1):e8511. doi:10.1371/journal.pone.0008511.
19. Kobayashi Y, Sanno Y, Sakai A, Sawabu Y, Tsutsumi M, Goto M, et al. Mathematical Modeling of Calcium Waves Induced by Mechanical Stimulation in Keratinocytes. *PLOS ONE*. 2014;9(3):e92650. doi:10.1371/journal.pone.0092650.
20. Kobayashi Y, Sawabu Y, Kitahata H, Denda M, Nagayama M. Mathematical Model for Calcium-Assisted Epidermal Homeostasis. *Journal of Theoretical Biology*. 2016;397:52–60. doi:10.1016/j.jtbi.2016.02.032.
21. Grabe N, Neuber K. A Multicellular Systems Biology Model Predicts Epidermal Morphology, Kinetics and Ca²⁺ Flow. *Bioinformatics*. 2005;21(17):3541–3547. doi:10.1093/bioinformatics/bti585.

22. Sütterlin T, Tsingos E, Bensaci J, Stamatias GN, Grabe N. A 3D Self-Organizing Multicellular Epidermis Model of Barrier Formation and Hydration with Realistic Cell Morphology Based on EPISIM. *Scientific Reports*. 2017;7:43472. doi:10.1038/srep43472.
23. Schaller G, Meyer-Hermann M. A Modelling Approach towards Epidermal Homeostasis Control. *Journal of Theoretical Biology*. 2007;247(3):554–573. doi:10.1016/j.jtbi.2007.03.023.
24. Miller C, Crampin E, Osborne JM. Maintaining the proliferative cell niche in multicellular models of epithelia. *Journal of Theoretical Biology*. Accepted for publication;.
25. Li X, Upadhyay AK, Bullock AJ, Dicolandrea T, Xu J, Binder RL, et al. Skin Stem Cell Hypotheses and Long Term Clone Survival – Explored Using Agent-Based Modelling. *Scientific Reports*. 2013;3:1904. doi:10.1038/srep01904.
26. Clayton E, Doupé DP, Klein AM, Winton DJ, Simons BD, Jones PH. A Single Type of Progenitor Cell Maintains Normal Epidermis. *Nature*. 2007;446(7132):185–189. doi:10.1038/nature05574.
27. Mascré G, Dekoninck S, Drogat B, Youssef KK, Brohé S, Sotiropoulou PA, et al. Distinct Contribution of Stem and Progenitor Cells to Epidermal Maintenance. *Nature*. 2012;489(7415):257–262. doi:10.1038/nature11393.
28. Sada A, Jacob F, Leung E, Wang S, White BS, Shalloway D, et al. Defining the Cellular Lineage Hierarchy in the Interfollicular Epidermis of Adult Skin. *Nature Cell Biology*. 2016;18(6):619–631. doi:10.1038/ncb3359.
29. Roberts D, Marks R. The Determination of Regional and Age Variations in the Rate of Desquamation: A Comparison of Four Techniques. *Journal of Investigative Dermatology*. 1980;74(1):13–16. doi:10.1111/1523-1747.ep12514568.
30. Bouwstra JA, de Graaff A, Gooris GS, Nijssse J, Wiechers JW, van Aelst AC. Water Distribution and Related Morphology in Human Stratum Corneum at Different Hydration Levels. *Journal of Investigative Dermatology*. 2003;120(5):750–758. doi:10.1046/j.1523-1747.2003.12128.x.
31. Kashibuchi N, Hirai Y, O’Goshi K, Tagami H. Three-Dimensional Analyses of Individual Corneocytes with Atomic Force Microscope: Morphological Changes Related to Age, Location and to the Pathologic Skin Conditions. *Skin Research and Technology*. 2002;8(4):203–211. doi:10.1034/j.1600-0846.2002.00348.x.
32. Menon GK. New Insights into Skin Structure: Scratching the Surface. *Advanced Drug Delivery Reviews*. 2002;54, Supplement:S3–S17. doi:10.1016/S0169-409X(02)00121-7.
33. Briggs GE, Haldane JBS. A Note on the Kinetics of Enzyme Action. *Biochemical Journal*. 1925;19(2):338–339. doi:10.1042/bj0190338.
34. Meineke FA, Potten CS, Loeffler M. Cell Migration and Organization in the Intestinal Crypt Using a Lattice-Free Model. *Cell Proliferation*. 2001;34(4):253–266.
35. Egawa M, Hirao T, Takahashi M. In Vivo Estimation of Stratum Corneum Thickness from Water Concentration Profiles Obtained with Raman Spectroscopy. *Acta Dermato-Venereologica*. 2007;87(1):4–8. doi:10.2340/00015555-0183.

36. Al-Amoudi A, Dubochet J, Norlén L. Nanostructure of the Epidermal Extracellular Space as Observed by Cryo-Electron Microscopy of Vitreous Sections of Human Skin. *Journal of Investigative Dermatology*. 2005;124(4):764–777. doi:10.1111/j.0022-202X.2005.23630.x.
37. Pathmanathan P, Cooper J, Fletcher A, Mirams G, Murray P, Osborne J, et al. A Computational Study of Discrete Mechanical Tissue Models. *Physical Biology*. 2009;6(3):036001. doi:10.1088/1478-3975/6/3/036001.
38. Atwell K, Qin Z, Gavaghan D, Kugler H, Hubbard EJA, Osborne JM. Mechano-Logical Model of *C. Elegans* Germ Line Suggests Feedback on the Cell Cycle. *Development*. 2015;142(22):3902–3911. doi:10.1242/dev.126359.
39. Mirams GR, Arthurs CJ, Bernabeu MO, Bordas R, Cooper J, Corrias A, et al. Chaste: An Open Source C++ Library for Computational Physiology and Biology. *PLoS Computational Biology*. 2013;9(3):e1002970. doi:10.1371/journal.pcbi.1002970.
40. Osborne JM, Fletcher AG, Pitt-Francis JM, Maini PK, Gavaghan DJ. Comparing Individual-Based Approaches to Modelling the Self-Organization of Multicellular Tissues. *PLoS Computational Biology*, Vol 13, Iss 2, p e1005387 (2017). 2017;13(2):e1005387. doi:10.1371/journal.pcbi.1005387.
41. Cooper FR, Baker RE, Bernabeu MO, Bordas R, Bowler L, Bueno-Orovio A, et al. Chaste: Cancer, Heart and Soft Tissue Environment. *Journal of Open Source Software*. 2020;5(47):1848. doi:10.21105/joss.01848.

Supporting information

S1 File. Subcellular model parameters. Sourcing and fitting the parameters for the subcellular model.

S2 File. Subcellular model results. Extended results for the subcellular model.

S1 Video. Healthy tissue video. Description of videos.

S2 Video. Treated tissue video *s*. Description of videos.

S3 Video. Treated tissue video *e*. Description of videos.